



Published in final edited form as:

*Adv Healthc Mater.* 2014 July ; 3(7): 1044–1052. doi:10.1002/adhm.201300519.

## Vaginal delivery of paclitaxel via nanoparticles with non-mucoadhesive surfaces suppresses cervical tumor growth

**Ming Yang,**

Center for Nanomedicine, Johns Hopkins University School of Medicine, 400 N Broadway, Baltimore MD 21231 (USA)

Department of Biomedical Engineering, Johns Hopkins University School of Medicine, 720 Rutland Avenue, Baltimore, MD 21205 (USA)

**Tao Yu,**

Center for Nanomedicine, Johns Hopkins University School of Medicine, 400 N Broadway, Baltimore MD 21231 (USA)

Department of Biomedical Engineering, Johns Hopkins University School of Medicine, 720 Rutland Avenue, Baltimore, MD 21205 (USA)

**Ying-Ying Wang,**

Center for Nanomedicine, Johns Hopkins University School of Medicine, 400 N Broadway, Baltimore MD 21231 (USA)

Department of Biomedical Engineering, Johns Hopkins University School of Medicine, 720 Rutland Avenue, Baltimore, MD 21205 (USA)

**Samuel K. Lai,**

Center for Nanomedicine, Johns Hopkins University School of Medicine, 400 N Broadway, Baltimore MD 21231 (USA)

Department of Chemical and Biomolecular Engineering, Johns Hopkins University, 3400 N Charles Street, Baltimore, MD 21218 (USA)

Eshelman School of Pharmacy, University of North Carolina at Chapel Hill, 120 Mason Farm Road, Chapel Hill, NC 27599 (USA)

**Qi Zeng,**

Department of Pathology, Johns Hopkins University School of Medicine, 600 N Wolfe Street, Baltimore, MD 21287 (USA)

**Bolong Miao,**

Department of Chemical and Biomolecular Engineering, Johns Hopkins University, 3400 N Charles Street, Baltimore, MD 21218 (USA)

**Benjamin C. Tang,**

---

\*hanes@jhu.edu.

M.Y. and T.Y. contributed equally to this work.

The terms of this arrangement are being managed by the Johns Hopkins University (J.H. and J.F.) in accordance with its conflict of interest policies.

Center for Nanomedicine, Johns Hopkins University School of Medicine, 400 N Broadway, Baltimore MD 21231 (USA)

Department of Chemical and Biomolecular Engineering, Johns Hopkins University, 3400 N Charles Street, Baltimore, MD 21218 (USA)

Koch Institute for Integrated Cancer Research, Massachusetts Institute of Technology, 77 Massachusetts Avenue, Cambridge, MA 02139 (USA)

**Brian W. Simons,**

Department of Molecular and Comparative Pathobiology, Johns Hopkins University School of Medicine, 1550 Orleans Street, Baltimore, MD, 21231 (USA)

**Laura Ensign,**

Center for Nanomedicine, Johns Hopkins University School of Medicine, 400 N Broadway, Baltimore MD 21231 (USA)

Department of Chemical and Biomolecular Engineering, Johns Hopkins University, 3400 N Charles Street, Baltimore, MD 21218 (USA)

Department of Ophthalmology, The Wilmer Eye Institute, Johns Hopkins University School of Medicine, 400 N. Broadway, Baltimore MD 21231 (USA)

**Guanshu Liu,**

F. M. Kirby Research Center for Functional Brain Imaging, Kennedy Krieger Institute, 707 N Broadway, Baltimore, MD, 21205 (USA)

The Russell H. Morgan Department of Radiology and Radiological Sciences, Johns Hopkins University School of Medicine, 600 N Wolfe Street, Baltimore, MD 21287 (USA)

**Kannie W. Y. Chan,**

F. M. Kirby Research Center for Functional Brain Imaging, Kennedy Krieger Institute, 707 N Broadway, Baltimore, MD, 21205 (USA)

The Russell H. Morgan Department of Radiology and Radiological Sciences, Johns Hopkins University School of Medicine, 600 N Wolfe Street, Baltimore, MD 21287 (USA)

**Chih-Yin Juang,**

Center for Nanomedicine, Johns Hopkins University School of Medicine, 400 N Broadway, Baltimore MD 21231 (USA)

**Olcay Mert,**

Department of Chemical and Biomolecular Engineering, Johns Hopkins University, 3400 N Charles Street, Baltimore, MD 21218 (USA)

**Joseph Wood,**

Department of Biomedical Engineering, Johns Hopkins University School of Medicine, 720 Rutland Avenue, Baltimore, MD 21205 (USA)

**Jie Fu,**

Center for Nanomedicine, Johns Hopkins University School of Medicine, 400 N Broadway, Baltimore MD 21231 (USA)

Department of Ophthalmology, The Wilmer Eye Institute, Johns Hopkins University School of Medicine, 400 N. Broadway, Baltimore MD 21231 (USA)

**Michael T. McMahon,**

Center for Nanomedicine, Johns Hopkins University School of Medicine, 400 N Broadway, Baltimore MD 21231 (USA)

F. M. Kirby Research Center for Functional Brain Imaging, Kennedy Krieger Institute, 707 N Broadway, Baltimore, MD, 21205 (USA)

The Russell H. Morgan Department of Radiology and Radiological Sciences, Johns Hopkins University School of Medicine, 600 N Wolfe Street, Baltimore, MD 21287 (USA)

**T.-C. Wu,**

Center for Nanomedicine, Johns Hopkins University School of Medicine, 400 N Broadway, Baltimore MD 21231 (USA)

Department of Pathology, Johns Hopkins University School of Medicine, 600 N Wolfe Street, Baltimore, MD 21287 (USA)

Department of Obstetrics and Gynecology, Johns Hopkins University School of Medicine, 600 N Wolfe Street, Baltimore, MD 21287 (USA)

Department of Oncology, Sidney Kimmel Comprehensive Cancer Center, Johns Hopkins University School of Medicine, 600 N Wolfe Street, Baltimore, MD 21287 (USA)

**Chien-Fu Hung, and**

Center for Nanomedicine, Johns Hopkins University School of Medicine, 400 N Broadway, Baltimore MD 21231 (USA)

Department of Pathology, Johns Hopkins University School of Medicine, 600 N Wolfe Street, Baltimore, MD 21287 (USA)

Department of Obstetrics and Gynecology, Johns Hopkins University School of Medicine, 600 N Wolfe Street, Baltimore, MD 21287 (USA)

Department of Oncology, Sidney Kimmel Comprehensive Cancer Center, Johns Hopkins University School of Medicine, 600 N Wolfe Street, Baltimore, MD 21287 (USA)

**Justin Hanes\***

Center for Nanomedicine, Johns Hopkins University School of Medicine, 400 N Broadway, Baltimore MD 21231 (USA)

Department of Biomedical Engineering, Johns Hopkins University School of Medicine, 720 Rutland Avenue, Baltimore, MD 21205 (USA)

Department of Chemical and Biomolecular Engineering, Johns Hopkins University, 3400 N Charles Street, Baltimore, MD 21218 (USA)

Department of Ophthalmology, The Wilmer Eye Institute, Johns Hopkins University School of Medicine, 400 N. Broadway, Baltimore MD 21231 (USA)

Department of Oncology, Sidney Kimmel Comprehensive Cancer Center, Johns Hopkins University School of Medicine, 600 N Wolfe Street, Baltimore, MD 21287 (USA)

Center for Cancer Nanotechnology Excellence, Institute for NanoBioTechnology, Johns Hopkins University, 3400 N Charles Street, Baltimore, MD 21218 (USA)

## Abstract

Local delivery of chemotherapeutics in the cervicovaginal tract using nanoparticles may reduce adverse side effects associated with systemic chemotherapy, while improving outcomes for early stage cervical cancer. We hypothesize drug-loaded nanoparticles must rapidly penetrate cervicovaginal mucus (CVM) lining the female reproductive tract to effectively deliver their payload to underlying diseased tissues in a uniform and sustained manner. We develop paclitaxel-loaded nanoparticles, composed entirely of polymers used in FDA-approved products, which rapidly penetrate human CVM and provide sustained drug release with minimal burst effect. We further employ a mouse model with aggressive cervical tumors established in the cervicovaginal tract to compare paclitaxel-loaded poly(lactic-co-glycolic acid) (PLGA) nanoparticles (conventional particles, or CP) and similar particles coated with Pluronic® F127 (mucus-penetrating particles, or MPP). CP are mucoadhesive and, thus, aggregated in mucus, while MPP achieve more uniform distribution and close proximity to cervical tumors. Paclitaxel-MPP suppress tumor growth more effectively and prolong median survival of mice compared to free paclitaxel or paclitaxel-CP. Histopathological studies demonstrate minimal toxicity to the cervicovaginal epithelia, suggesting paclitaxel-MPP may be safe for intravaginal use. These results demonstrate for the first time the *in vivo* advantages of polymer-based MPP for treatment of tumors localized to a mucosal surface.

## Keywords

drug delivery; cancer; controlled release; chemotherapy; biodegradable polymers; Biomedical Applications; Nanoparticles

## 1. Introduction

The vast majority of cervical cancer patients are diagnosed at early stages of the disease, when tumors are confined to the cervix (Stage I) and remain small in size.<sup>[1]</sup> Nevertheless, current standards of care for early stage cervical cancer generally fail to eradicate tumors without significant adverse side effects: both surgery (excisional or ablative procedures) and radiation therapy are associated with increased risks for future negative gynecological and obstetric outcomes, such as impaired sexual function, infertility, preterm delivery and low birth weight.<sup>[2]</sup> Systemic chemotherapy represents a third treatment option. However, systemically administered drugs reach mucosal tissues, such as the epithelial surface of the cervix, with very low efficiency. Thus, even high doses of chemotherapy typically fail to elicit therapeutic responses, while causing significant systemic toxicity.<sup>[3]</sup> For these reasons, systemic chemotherapy is generally the last option for cervical cancer treatment, and is often used only concurrently with other treatments; it is rarely used for early stage disease.

Methods that enable sustained and localized chemotherapy delivery in the female reproductive tract may reduce the adverse side effects commonly associated with systemic chemo, while improving efficacy by providing higher drug concentrations at the tumor site

over prolonged periods of time. However, the cervicovaginal (CV) epithelium is highly permeable,<sup>[4]</sup> which not only limits the duration over which an adequate drug concentration can be maintained locally, but also increases the likelihood of adverse systemic side effects, particularly when higher dosages and/or repeated administration are needed. The high permeability of the CV epithelium also likely contributes to the poor distribution of topically administered free drugs, as previously demonstrated for various vaginal microbicides.<sup>[5]</sup> Thus, vaginal instillation of unencapsulated chemo drugs is expected to provide minimal therapeutic efficacy, and may cause significant systemic toxicity.

Nanoparticle-based drug and gene delivery systems have gained increasing interest for their potential therapeutic or prophylactic applications in the female reproductive tract. A number of nanoparticle-based platforms, including polymeric nanoparticles,<sup>[6]</sup> and quantum dots,<sup>[7]</sup> have been developed that show potential in animal models for preventing sexually transmitted infections,<sup>[8]</sup> prophylaxis against the development of cervicovaginal tumors,<sup>[9]</sup> and improved siRNA delivery<sup>[10]</sup>. However, conventional polymeric nanoparticles, including those composed of polymers used in FDA-approved products, poly(lactic-co-glycolic acid) (PLGA) and polycaprolactone, are easily immobilized by the viscoelastic and adhesive cervicovaginal mucus (CVM) secretions coating the CV epithelium.<sup>[6a-c, 11]</sup> These conventional particles (CP) not only suffer from poor distribution in the CV tract, but also are unlikely to access the deeper, more slowly cleared mucus layers near the epithelium for prolonged retention and drug release.<sup>[8]</sup>

To address the limitations of mucosal drug delivery with standard polymer nanoparticles, we developed “mucus-penetrating particles” (MPP) by coating nanoparticles with an exceptionally dense layer of low MW poly(ethylene glycol) (PEG).<sup>[6a-c, 11-12]</sup> PEG is a hydrophilic and uncharged polymer, which at sufficiently dense coverage can effectively minimize adhesive interactions between nanoparticles and anionic glycans or periodic hydrophobic naked protein domains on mucins.<sup>[12-13]</sup> Furthermore, we recently developed a simple non-covalent coating process to produce MPP composed entirely of GRAS (Generally Regarded As Safe by the FDA) materials.<sup>[6b]</sup> Here, we report the formulation of an all GRAS, paclitaxel (PTX)-loaded drug carrier, composed of PLGA and Pluronic<sup>®</sup> F127, that rapidly penetrates human CVM *ex vivo* and enhances the efficacy of PTX against tumors in the reproductive tract of female mice.

## 2. Results and Discussion

### 2.1. Characterization of PTX-loaded nanoparticles and drug release *in vitro*

To develop a drug-loaded MPP system for potential treatment of cervical cancer, we formulated nanoparticles composed of PLGA and Pluronic<sup>®</sup> F127 encapsulating PTX, a frontline chemotherapeutic drug, by a nanoprecipitation method. Scanning electron micrographs showed that both PLGA MPP encapsulating PTX (PTX/MPP) and the corresponding conventional PLGA particles (formulated without F127; PTX/CP) possessed smooth surfaces and a relatively uniform size distribution, with no visible drug precipitates or impurities (Figure 1a,b). The narrow size distributions of PTX/MPP and PTX/CP were confirmed by dynamic light scattering, with average diameters of 239 and 234 nm, respectively (Table 1). The drug loading of PTX/MPP (~ 5% w/w) was comparable to that

of PTX/CP (~ 8%) (Table 1). We also characterized the *in vitro* release of encapsulated PTX from PTX/MPP and PTX/CP at pH 7.4 and 37°C; both particle types released PTX in a similar fashion over 3 days with minimal burst release (Figure 1c). In general, PTX/MPP and PTX/CP showed similar physical characteristics, and provided sustained release of PTX at comparable rates.

## 2.2. PTX/MPP rapidly penetrate human CVM

To test whether PTX/MPP were capable of diffusing rapidly in mucus secretions, we measured their transport rates in human CVM using multiple particle tracking.<sup>[11, 14]</sup> The time-lapse traces of PTX/MPP in CVM resembled unobstructed Brownian motion (Figure 2a); in contrast, the trajectories of PTX/CP in the same CVM samples were highly constrained and non-Brownian (Figure 2b). We quantified particle transport rates in the form of an ensemble-averaged geometric mean squared displacement ( $\langle \text{MSD} \rangle$ ), and found that the  $\langle \text{MSD} \rangle$  of PTX/MPP was > 6,500-fold higher than that of PTX/CP at a time scale of 1s (Figure 2c). Overall, PTX/CP were slowed on average > 40,000-fold in CVM compared to their theoretical speeds in water, whereas PTX/MPP were slowed only 6-fold (Table 1). The distributions of the logarithms of individual particle effective diffusivities showed the greater ensemble average mobility of PTX/MPP was due to a near-uniform increase in particle speeds for PTX/MPP compared to PTX/CP, and not due to a small fraction of fast moving outlier nanoparticles (Figure 2d).

The average size of PTX/MPP and PTX/CP was 230–240 nm, smaller than the average mesh size of the mucin network in human CVM (estimated average ~ 340 nm, with 80% of pores larger than 200 nm in diameter<sup>[15]</sup>). Thus, steric exclusion of both types of particles by the mucus gel should be minimal. The greatly improved mobility of PTX/MPP compared to PTX/CP in human CVM may therefore be attributed largely to the formation of an effective muco-inert shield by surface-coated F127. The surface charge and mobility of PTX/MPP were comparable to those of similarly sized blank MPP reported previously,<sup>[6b]</sup> suggesting the incorporation of PTX did not interfere with surface coating by F127.

## 2.3. Characterization of intravaginal cervical tumor model by bioluminescence and magnetic resonance imaging (MRI)

A key challenge to demonstrating improved *in vivo* efficacy by MPP is the choice of an animal model that features a mucus barrier to allow differentiation of the *in vivo* performance of MPP vs. CP. Here, we employed a tumor model of cervical cancer established by locally implanting TC-1 tumor cells in the mouse vagina,<sup>[16]</sup> which has a CVM layer. TC-1 cells, genetically modified to express luciferase enzyme,<sup>[17]</sup> were applied intravaginally, allowing the cells to attach to and proliferate in the CV epithelium. MRI has been used previously to delineate cervical cancer based on its superb soft tissue contrast,<sup>[18]</sup> and we employed T2-weighted anatomical MRI to confirm tumor implantation and to evaluate the progress of tumor growth. TC-1 tumors grew along the length of the CV tract and extended laterally toward surrounding tissues (Figure 3a–c). We also quantified tumor growth via bioluminescence imaging on live animals and characterized physical tumor weight at predetermined intervals. We found a near linear correlation between the bioluminescence signal and tumor weight (Figure 3d), suggesting the bioluminescent TC-1

tumor model affords accurate assessment of tumor size. This enables high-throughput longitudinal monitoring of tumor growth in the same mice in a non-invasive fashion.

The TC-1 model offers a number of desirable features for the current study. TC-1 cells are immortalized murine epithelial cells that were transformed to express HPV-16 E6/E7 and activated human c-Ha-ras oncogene, i.e., they exhibit similar genetic traits as human papillomavirus (HPV)-induced cervical tumors.<sup>[19]</sup> We previously showed that the TC-1 model also recapitulates many of the aspects of cervical cancer tumor progression in the cervicovaginal tract.<sup>[16]</sup> These cells consistently produce highly aggressive tumors, and are thus a stringent model for testing new therapeutic approaches within a short time frame. Finally, the localization of tumors to the mouse CV tract not only resembles the anatomy of the human disease, but also features a CVM layer that acts as a barrier to particle penetration, making this model well-suited for testing whether muco-inert MPP may provide more effective drug delivery *in vivo* than mucoadhesive CP.

#### 2.4. MPP distribute more uniformly than CP in the mouse CV tract

We next sought to determine whether the ability of PTX/MPP to penetrate human CVM *ex vivo* may lead to improved particle penetration across the protective mucus layer in the mouse vagina, as compared to PTX/CP. We administered fluorescently labeled MPP or CP suspension to the vaginas of mice bearing TC-1 tumors, and harvested the entire vagina from each mouse after 20 hr. Fluorescent images of transverse cross-sections of vaginal tissue show that CP aggregated and remained localized in the lumen of the vagina, failing to penetrate the mucus barrier and reach tumors (Figure 4a). In contrast, MPP remained well-dispersed and distributed uniformly, including in close proximity to the epithelial surface and tumors (Figure 4b).

We previously demonstrated that enhanced mucus penetration can lead to improved distribution of MPP over the mucosal surface of a healthy mouse vaginal tract.<sup>[8]</sup> Our results here confirm that MPP also spread more uniformly than CP in mice bearing vaginal tumors. The uniform distribution of MPP over the epithelial surface may allow the particles to achieve a higher concentration of PTX in closer proximity to tumors, which may more effectively suppress tumor growth. In contrast, CP aggregated in the vaginal lumen, likely due to their strong mucoadhesive properties,<sup>[8]</sup> preventing them from reaching tumor tissues and precluding sustained drug release in proximity to tumors. Aggregation of CP in mucus may also reduce the amount of drug released over time due to a lower effective surface area,<sup>[20]</sup> potentially further reducing the therapeutic efficacy of CP.

#### 2.5. PTX/MPP provide sustained drug retention in the mouse CV tract

When delivered topically in the CV tract, Taxol<sup>®</sup>, the clinical formulation of PTX dissolved in Cremophor<sup>®</sup>/ethanol, is readily eliminated due to systemic absorption across the highly permeable vaginal epithelium. We therefore sought to determine whether PTX/MPP can prolong drug retention in the mouse CV tract compared to Taxol<sup>®</sup> administered intravaginally (local Taxol<sup>®</sup>) or intraperitoneally (systemic Taxol<sup>®</sup>), by quantifying PTX extracted from the mouse CV tract over time (Figure 5). In the local Taxol<sup>®</sup> group, the amount of drug in the CV tract decreased rapidly to ~ 14% of the initial dose by 4 hr, and

only ~ 1% of the initial dose by 24 hr. In contrast, in the PTX/MPP group, the amount of retained drug, in the form of both released drug and encapsulated drug in PTX/MPP, decreased at a much slower rate, with ~ 70% of the initial dose remaining 24 hr post-administration. In the systemic Taxol<sup>®</sup> group, drug levels were below the detection limit at all time points, suggesting a limited amount of drug reached the CV tract through systemic circulation. The prolonged retention of PTX by PTX/MPP may be attributed to the slow elimination of MPP by mucus clearance,<sup>[8]</sup> as well as the sustained release of drugs from the particles. Sustained retention of PTX provided by MPP may enhance tumor suppression by maintaining a stable, therapeutically effective level of PTX at tumor sites, which is not achievable by local or systemic Taxol<sup>®</sup>.

## 2.6. PTX/MPP effectively suppress tumor growth in the mouse CV tract

We next evaluated the therapeutic efficacy of PTX/MPP compared to PTX/CP and Taxol<sup>®</sup> in our cervicovaginal tumor model. Beginning 3 days after tumor inoculation, mice were treated daily with an intravaginal dose of PTX/MPP, PTX/CP or Taxol<sup>®</sup>, each at 3 mg/kg of PTX. Tumors in the control group grew rapidly without treatment (Figure 6a). By Day 11, the total tumor load, as reflected by bioluminescence measurements, was 115-fold higher than that at Day 3. The tumor growth rate in the local Taxol<sup>®</sup> group was slightly slower, with an overall tumor load equal to ~ 60% of the control group by Day 11. PTX/CP exhibited slightly improved efficacy compared to local Taxol<sup>®</sup>, with an average bioluminescence signal of ~ 42% that of the control group at Day 11. In contrast, the tumor load for the PTX/MPP group was only ~ 7% that of the control group at Day 11, statistically lower than that of any other group ( $p < 0.05$ ). Based on Kaplan-Meier survival curves, local Taxol<sup>®</sup> and PTX/CP only extended the median survival time to 11 days vs. 9 days for the untreated control group, a difference that was not statistically significant (Figure 6b). In comparison, PTX/MPP doubled the median survival time to 19 days, a result that was statistically significant compared to all other treatment groups.

Since PTX/CP exhibited a similar size distribution and drug release profile as PTX/MPP, the lower efficacy of PTX/CP against cervical tumors was likely due to their inability to penetrate mucus. In contrast, PTX/MPP were able to penetrate the mucus layer lining the vaginal epithelium, thereby achieving a more uniform distribution and maintaining an elevated and sustained level of PTX in close proximity to tumors. These factors likely contribute critically to improved suppression of tumor growth by MPP in the aggressive TC-1 tumor model. MPP may also enhance suppression of other tumors localized to mucosal surfaces, such as early-stage lung or colorectal tumors, where mucus serves as a critical barrier to locally delivered therapeutics. In addition, the therapeutic advantages of MPP may be even more pronounced in cancers with abnormally elevated mucus secretion, for example, in adenocarcinomas.

It should be noted that the TC-1 tumor model is very aggressive, with tumor volume reaching 2,000 mm<sup>3</sup> in less than 30 days if left untreated.<sup>[16]</sup> In comparison, other cervical cancer models, such as transgenic models requiring sophisticated genetic modifications,<sup>[9, 21]</sup> models induced by vaginally administered carcinogen,<sup>[22]</sup> or models involving surgically implanted tumor xenografts,<sup>[23]</sup> usually take much longer to establish.

While the fast establishment of TC-1 tumors enables efficient evaluation of new chemotherapeutic systems, the aggressiveness of tumor growth also makes complete suppression unlikely. As tumor size increases over time, the ability of drugs to penetrate into the tumor likely decreases. Elevated interstitial pressure within tumor tissue significantly reduces convection-driven transport of drug molecules into tumors.<sup>[24]</sup> In addition, binding to tissue elements, drug metabolism and systemic absorption further reduce effective diffusion of drug within tumor tissue.<sup>[25]</sup> Although the drugs may kill superficial layers of tumor cells, their inability to penetrate into the tumor core may prevent complete eradication of the tumor.<sup>[25]</sup> Thus, long-term survival of mice using the TC-1 model is very difficult to achieve. Nevertheless, it is likely that PTX/MPP may more effectively suppress, or perhaps even eradicate, early stage tumors in humans, which are typically much less aggressive than TC-1 and progress much more slowly.<sup>[26]</sup> Future studies using alternative murine cervical tumor models that are less aggressive and better resemble the slow tumor progression in humans<sup>[9, 21–23]</sup> may further substantiate the effectiveness of PTX/MPP.

### 2.7. PTX/MPP are well tolerated in the mouse CV tract

Finally, vaginal histology was assessed for mice receiving the various treatment options at 24 and 48 hr after treatment (Figure 7). Overall, minimal toxicity was observed in all groups, with no evidence of abnormal epithelial exfoliation or erosion and, at most, mild inflammatory cell infiltrates. Compared to systemic Taxol<sup>®</sup>, all local treatment groups (PTX/MPP, PTX/CP and local Taxol<sup>®</sup>) showed slightly greater cytotoxicity, consistent with the higher local concentration of PTX. At 24 hr after treatment, changes in nuclear morphology (chromatin clumping, nuclear fragmentation) were evident in a minority of vaginal epithelial cells, and particularly basal cells, for all local treatment conditions. Similarly, a slight increase in the number of apoptotic epithelial cells was noted after 48 hr in all three groups treated intravaginally compared to mice treated with systemic Taxol<sup>®</sup>. Both PTX/MPP and PTX/CP groups showed minimal to mild inflammatory cell infiltrate at 24 hr, which resolved by 48 hr. Systemic Taxol<sup>®</sup> and local Taxol<sup>®</sup> groups showed no increase in inflammation above background level. Histology of all intravaginally treated groups was normal at 6 days after treatment. These results indicate vaginal PTX/MPP treatment was well-tolerated with no severe adverse effects in the mouse CV tract.

In contrast to polymeric particles composed of PEG-containing block copolymers or pre-fabricated particles with covalently attached PEG coatings, Pluronic-coated particles, such as the PLGA/F127 MPP system described here, do not generate any covalent linkages that would constitute a new chemical entity to the FDA. Thus, the safety profile of the particles is likely equivalent to those of its components, PLGA and Pluronic, both of which are well known for their biocompatibility and use in a broad range of FDA-approved pharmaceutical products.<sup>[6b, 27]</sup> We expect that the all-GRAS nature of the PLGA/F127 system will facilitate faster, more economical, and more scalable translation to human clinical trials.

## 3. Conclusions

In this study, we developed a drug-encapsulated polymer-based MPP platform entirely composed of materials used in FDA-approved products, and showed that MPP released drug

continuously over 3 days *in vitro*. MPP remained well-dispersed and distributed uniformly across the vaginal mucosal surface, achieving close proximity to tumors established in the mouse CV tract. Local PTX/MPP suppressed the growth of aggressive cervical tumors and prolonged the median survival of mice more effectively than local PTX/CP or free Taxol<sup>®</sup>. To our knowledge, this is the first demonstration that polymer-based MPP can provide enhanced efficacy in an *in vivo* disease model. We expect that the biodegradable MPP platform can be adapted to deliver a variety of therapeutics and, compared to conventional mucoadhesive particles, achieve improved distribution and efficacy at other mucosal surfaces, making them promising candidates for treating cancers localized to the mucosae.

## 4. Experimental

### Nanoparticle preparation and characterization

PTX/MPP were prepared using a nanoprecipitation method similar to that previously described.<sup>[6b, 28]</sup> Briefly, PLGA (15 kDa, L:G ratio ~ 50%:50%; SurModics Pharmaceuticals, Inc., Birmingham, AL) and PTX (LC Laboratories, Woburn, MA) were co-dissolved in acetonitrile (20 and 4mg/mL), respectively, and the polymer and drug solution (1 mL) was added dropwise into Pluronic<sup>®</sup> F127 (BASF, Florham Park, NJ) solution (40 mL, 10% w/v). PTX/CP were similarly prepared, and poly(vinyl alcohol) (PVA, 25 kDa; Polysciences, Inc., Warrington, PA) was used in place of F127 to facilitate PTX encapsulation. After stirring for 2 hr to remove the organic solvent, the nanoparticles were collected by centrifugation at 11,648 ×g (Sorvall Legend X1R centrifuge; Thermo Fisher Scientific Inc., Asheville, NC) for 20 min, washed twice, and used within 2 hr. To characterize particle transport in human CVM, doxorubicin (NetQem, Durham, NC), intrinsically fluorescent with excitation/emission maxima at 480/550 nm, was chemically conjugated to PLGA as previously described.<sup>[29]</sup> Fluorescent PTX-loaded nanoparticles were prepared following similar procedures to those described above using doxorubicin-labeled PLGA. Particles formulated to assess *in vivo* distribution were prepared similarly but without PTX or additional stabilizers besides F127. Doxorubicin-labeled PLGA was only used to formulate particles for studies requiring observation of particles by fluorescence microscopy (particle tracking and *in vivo* distribution, but not *in vivo* particle retention and efficacy against cervical tumors). Size and ζ-potential of nanoparticles were determined by dynamic light scattering and laser Doppler electrophoresis, respectively, using a Zetasizer NanoZS90 (Malvern Instruments, Southborough, MA) following manufacturer instructions. Particle morphology was characterized by scanning electron microscopy (SEM) using a cold cathode field emission SEM (JEOL JSM-6700F, Peabody, MA). Nanoparticles were lyophilized, resuspended in ethanol (100%) and dried onto SEM mounts at room temperature. Particles were then sputter coated with platinum prior to imaging.

### Characterization of drug loading and *in vitro* drug release profile

PTX/MPP and CP were lyophilized and subsequently dissolved in acetonitrile to extract PTX. After centrifugation (15,000 ×g, 5 min) and filtration through a 0.2 μm PTFE filter, the filtrate (50 μL) was injected into a Shimadzu High Performance Liquid Chromatography (HPLC) system equipped with a C18 reverse phase column (5 μm, 4.6×250 mm; Varian Inc., Santa Clara, CA). PTX was eluted using an isocratic mobile phase containing water

and acetonitrile (35%:65%, v/v) at 1 mL/min and detected at 229 nm using a UV detector. The data was analyzed using LCsolution software (Shimadzu Scientific Instruments, Columbia, MD). Drug loading was defined as the weight ratio of drug to polymer. To determine the drug release kinetics of the nanoparticles, 10 mg of PTX/MPP or CP was suspended in PBS (40 mL, pH = 7.4), and octanol (5 mL) was added on top of the PBS, as described previously.<sup>[30]</sup> At pre-determined time intervals, the octanol phase was collected and replaced with fresh octanol. Quantitative analysis of released drug was performed using HPLC after a 1:2 (v/v) dilution of the octanol release samples with acetonitrile. The data was analyzed using LCsolution software.

### High resolution multiple particle tracking

Human CVM was collected as previously described,<sup>[11]</sup> following a protocol approved by the Johns Hopkins School of Medicine Institutional Review Board. Collected mucus samples were stored at 4 °C until used for microscopy within 4 hr. Suspensions of fluorescently labeled nanoparticles (~ 10<sup>10</sup> particles/mL) were added at 3% v/v to human CVM (20 µL) and samples were incubated 1 hr at 37 °C before microscopy. Particle transport rates were measured by analyzing trajectories of fluorescent particles, recorded using a silicon-intensified target camera (VE-1000; Dage-MTI, Michigan, IN) mounted on an inverted epifluorescence microscope equipped with a 100× oil-immersion objective (numerical aperture 1.3). Movies were captured using MetaMorph software (Molecular Devices, Inc., Sunnyvale, CA) at a temporal resolution of 66.7 ms for 20 s. The tracking resolution was 10 nm, as determined by tracking the displacements of particles immobilized with a strong adhesive.<sup>[11]</sup> Trajectories of  $n > 100$  particles were analyzed for each experiment, and three experiments in CVM from different donors were performed for each condition. The coordinates of nanoparticle centroids were transformed into time-averaged mean squared displacements (MSD),  $\langle r^2(\tau) \rangle = [x(t + \tau) - x(t)]^2 + [y(t + \tau) - y(t)]^2$  ( $\tau$  = time scale or time lag), from which distributions of MSDs and effective diffusivities were calculated.<sup>[11, 14]</sup> The theoretical diffusivities of nanoparticles in water were calculated from the Stokes-Einstein equation,  $D_w = k_B T / 6\pi\eta R$ , where the Boltzmann constant  $k_B = 1.38 \times 10^{-23} \text{ m}^2 \cdot \text{kg} \cdot \text{s}^{-2} \cdot \text{K}^{-1}$ ,  $T = 293.15 \text{ K}$ , the viscosity of water  $\eta = 0.001 \text{ Pa} \cdot \text{s}$ , and  $R$  as the diameter of the nanoparticles.

### Cervicovaginal tumor model and treatment

All experiments conducted with mice were performed in accordance with protocols approved by the Johns Hopkins University Animal Care and Use Committee satisfying the requirements of the E.E.C. Guidelines (1986) and U.S. Federal Guidelines (1985). C57BL/6 mice (6–8 weeks old) were treated with Depo-Provera<sup>®</sup> (medroxyprogesterone acetate, 2.5 mg/mouse) by subcutaneous injection into the right flank ~ 7 days prior to use. For tumor inoculation, mice were anesthetized, and their cervicovaginal epithelia gently disrupted using cytobrushes, before TC-1 tumors cells expressing luciferase were inoculated by vaginal instillation ( $1 \times 10^5$  cells per mouse).<sup>[16]</sup> Tumor growth was monitored by live animal bioluminescence imaging, and anatomical MRI was also performed ~ 7 days after tumor inoculation to assess tumor growth. Detailed information on MRI analysis is described in a different section. Beginning 3 days after tumor challenge, mice were treated daily with an intravaginal dose (3 mg/kg) of PTX/MPP, PTX/CP or free drug ( $n = 5-6$  mice

per condition, mice were grouped to have similar starting levels of bioluminescence signals). Mice were prevented from self-grooming following each treatment for ~ 12 hours by a collar.<sup>[8]</sup> Mice with no treatment served as a negative control. Tumor growth was monitored by live animal bioluminescence imaging at different time points. Bioluminescence signals were analyzed using Living Image software (Caliper Life Sciences, Inc., Hopkinton, MA). In brief, a circular region of interest (ROI) that includes the entire vaginal region was created for each mouse, and its bioluminescence signal was measured as total photon flux (p/s, photons per second). The same ROI size was used among all mice to ensure consistency. For Kaplan-Meier survival curves, mice were excluded once the bioluminescence signal reached  $5 \times 10^7$  p/s as an indication of disease advancement.

### Characterization of intravaginal cervical tumor model by MRI

To assess tumor growth, T2-weighted MR images were acquired ~ 7 days after tumor inoculation using a 9.4T horizontal bore small animal scanner (Bruker BioSpin Corp., Billerica, MA) equipped with a 25 mm sawtooth resonator. In brief, a modified Rapid Acquisition with a modified Relaxation Enhancement (RARE) sequence including a fat suppression pulse (3.4 ms hermite pulse, offset = -3.5 ppm) was used to acquire the MR images. The acquisition parameters were: TR = 3.0 s, effective TE = 18 ms, RARE factor = 8, slice thickness = 0.7 mm, acquisition matrix size = 256×128, in plane resolution = 167  $\mu$ m × 142  $\mu$ m, and single acquisition (NA = 1). Multi-slice MR images were acquired along three dimensions (coronal, sagittal and axial) of the CV tract.

### Distribution of nanoparticles in the mouse vagina

To evaluate nanoparticle distribution *in vivo*, 5  $\mu$ L of fluorescently labeled PLGA CP or MPP suspension were administered intravaginally to mice bearing CT-1 tumors. After 20 hr, the entire vagina was gently removed and frozen in Tissue-Tek<sup>®</sup> O.C.T.<sup>™</sup> Compound (Sakura Finetek U.S.A., Inc., Torrance, CA). Transverse sections were obtained at various points along the length of the tissue (between the introitus and the cervix) using a Leica Cryostat (Leica Microsystems Inc., Bannockburn, IL). The thickness of the sections was set to 50  $\mu$ m to minimize possible artifacts due to displacement of mucus and particles. Fluorescent images of the sections were obtained using a LSM 510 confocal laser scanning microscope (Carl Zeiss Inc., Thornwood, NY). Images in Figure 4 are representative of the observations from 3 mice per particle type.

### Retention of PTX in the mouse vagina

To evaluate the retention of PTX delivered in PTX/MPP or as free drug in the mouse vagina quantitatively, we administered PTX/MPP and free Taxol<sup>®</sup> (clinical formulation of PTX) intravaginally, with free Taxol<sup>®</sup> administered intraperitoneally as a systemic treatment for comparison to local treatments. Mice were prevented from self-grooming through the entire course of the study (24 hours) by an Elizabethan collar. At select time points up to ~ 24 hr, mice were given 10× vaginal lavage with 30  $\mu$ L of normal saline. The entire vagina was then collected and treated with cell lysis buffer. The lavage and vaginal tissue samples were lyophilized and acetonitrile was used to dissolve PTX in the lyophilized samples. The amount of drug in each sample was quantified by HPLC.

## Assessment of intravaginal toxicity

To assess the toxicity caused by different treatments, PTX was administered intravaginally or systemically at a dose of 3 mg/kg as free drug or encapsulated in PLGA nanoparticles (n = 5 mice per treatment group). At the indicated times after dosing, mice were sacrificed and the CV tissues collected. After fixation in neutral buffered formalin solution (10%), the tissue samples were routinely processed and embedded in paraffin wax. For histological analysis, 5 µm thick sections were taken at 100 µm intervals, and stained with hematoxylin and eosin. Two sections from each mouse were reviewed in a blinded fashion by a pathologist and scored in a semi-quantitative fashion according to established guidelines for evaluating vaginal toxicity/irritation [31], modified to include assessment for toxic effects of Taxol®. Sections were evaluated for multiple injury parameters including leukocyte infiltration, epithelial exfoliation, vascular congestion and edema. Polymorphonuclear leukocyte infiltration was identified by the characteristic multi-lobed nuclei of these inflammatory cells. Pyknotic and apoptotic cells were identified by condensed, hyperchromatic or fragmented nuclei and shrunken, eosinophilic cytoplasm.

## Statistical analysis

All data are presented as a mean with standard error of the mean (S.E.M.) indicated. Statistical significance of *in vivo* drug retention values (Figure 5) was performed using one way analysis of variance (ANOVA) followed by Tukey's test. Differences in tumor burden (Figure 6a) and survival (Figure 6b) between treatment groups were evaluated using a Kruskal-Wallis ANOVA and a Log-rank (Mantel-Cox) test, respectively. All other statistical analyses were performed using one-tailed Student's *t*-tests, assuming unequal variance. *P*-values < 0.05 were considered statistically significant.

## Acknowledgments

We would like to thank Mr. Mark Koontz for his help with scanning electron microscopy. This work was supported in part by NIH grants R01CA140746 (J.H.), U54CA151838 (J.H.), P50CA098252 (T.W.), R01CA114425 (T.W.) and R01EB015031 (M.T.M.), and National Science Foundation Graduate Research Fellowships (Y.-Y.W. and L.E.). The content is solely the responsibility of the authors and does not necessarily represent the official views of the National Cancer Institute, the National Institute of Allergy and Infectious Diseases, or the National Institute of Biomedical Imaging and Bioengineering. The mucus-penetrating particle technology described in this publication is being developed by Kala Pharmaceuticals. J.H. is co-founder and consultant to Kala. J.H. and J.F. own company stock, which is subject to certain restrictions under University policy.

## References

1. Creasman WT. *Gynecol Oncol.* 1995; 58:157. [PubMed: 7622099]
2. a) Jensen PT, Groenvold M, Klee MC, Thranov I, Petersen MA, Machin D. *Cancer.* 2004; 100:97. [PubMed: 14692029] b) Kyrgiou M, Koliopoulos G, Martin-Hirsch P, Arbyn M, Prendiville W, Paraskevaidis E. *Lancet.* 2006; 367:489. [PubMed: 16473126]
3. Allen TM, Cullis PR. *Science.* 2004; 303:1818. [PubMed: 15031496]
4. a) Forsberg JG. *Acta Obstet Gynecol Scand Suppl.* 1996; 163:3. [PubMed: 8916469] b) Rayburn WF, Powers BL, Plasse TF, Carr D, Di Spirito M. *J Soc Gynecol Investig.* 2006; 13:112.
5. Cone RA, Hoen T, Wong X, Abusuwwa R, Anderson DJ, Moench TR. *BMC Infect Dis.* 2006; 6:90. [PubMed: 16740164]
6. a) Tang BC, Dawson M, Lai SK, Wang YY, Suk JS, Yang M, Zeitlin P, Boyle MP, Fu J, Hanes J. *Proc Natl Acad Sci U S A.* 2009; 106:19268. [PubMed: 19901335] b) Yang M, Lai SK, Wang YY, Zhong W, Happe C, Zhang M, Fu J, Hanes J. *Angew Chem Int Ed Engl.* 2011; 50:2597. [PubMed:

- 21370345] c) Yu T, Wang YY, Yang M, Schneider C, Zhong W, Pulicare S, Choi WJ, Mert O, Fu J, Lai SK, Hanes J. *Drug Deliv Transl Res.* 2012;2.d) Cu Y, Saltzman WM. *Mol Pharm.* 2009; 6:173. [PubMed: 19053536] e) Cu Y, Booth CJ, Saltzman WM. *J Control Release.* 2011; 156:258. [PubMed: 21763739]
7. Ballou B, Andreko SK, Osuna-Highley E, McRaven M, Catalone T, Bruchez MP, Hope TJ, Labib ME. *PLoS One.* 2012; 7:e51995. [PubMed: 23284844]
  8. Ensign LM, Tang BC, Wang YY, Tse TA, Hoen T, Cone R, Hanes J. *Sci Transl Med.* 2012; 4:138ra79.
  9. Blum JS, Weller CE, Booth CJ, Babar IA, Liang X, Slack FJ, Saltzman WM. *Drug Deliv Transl Res.* 2011; 1:383.
  10. Woodrow KA, Cu Y, Booth CJ, Saucier-Sawyer JK, Wood MJ, Saltzman WM. *Nat Mater.* 2009; 8:526. [PubMed: 19404239]
  11. Lai SK, O'Hanlon DE, Harrold S, Man ST, Wang YY, Cone R, Hanes J. *Proc Natl Acad Sci U S A.* 2007; 104:1482. [PubMed: 17244708]
  12. Wang YY, Lai SK, Suk JS, Pace A, Cone R, Hanes J. *Angew Chem Int Ed Engl.* 2008; 47:9726. [PubMed: 18979480]
  13. Lai SK, Wang YY, Hanes J. *Adv Drug Deliv Rev.* 2009; 61:158. [PubMed: 19133304]
  14. Suh J, Wirtz D, Hanes J. *Biotechnol Prog.* 2004; 20:598. [PubMed: 15059007]
  15. Lai SK, Wang YY, Hida K, Cone R, Hanes J. *Proc Natl Acad Sci U S A.* 2010; 107:598. [PubMed: 20018745]
  16. Zeng Q, Peng S, Monie A, Yang M, Pang X, Hung CF, Wu TC. *Hum Gene Ther.* 2011; 22:809. [PubMed: 21128743]
  17. Kim D, Hung CF, Wu TC. *Hum Gene Ther.* 2007; 18:575. [PubMed: 17576157]
  18. a) Burghardt E, Hofmann HM, Ebner F, Haas J, Tamussino K, Justich E. *Gynecol Oncol.* 1989; 33:61. [PubMed: 2703168] b) Garbow JR, Santeford AC, Anderson JR, Engelbach JA, Arbeit JM. *Cancer Res.* 2009; 69:7945. [PubMed: 19789343] c) Togashi K, Nishimura K, Itoh K, Fujisawa I, Asato R, Nakano Y, Itoh H, Torizuka K, Ozasa H, Mori T. *Radiology.* 1986; 160:431. [PubMed: 3726122]
  19. Lin KY, Guarnieri FG, Staveley-O'Carroll KF, Levitsky HI, August JT, Pardoll DM, Wu TC. *Cancer Res.* 1996; 56:21. [PubMed: 8548765]
  20. a) Ostacolo L, Marra M, Ungaro F, Zappavigna S, Maglio G, Quaglia F, Abbruzzese A, Caraglia M. *J Control Release.* 2010; 148:255. [PubMed: 20816710] b) Fukuda M, Miller DA, Peppas NA, McGinity JW. *Int J Pharm.* 2008; 350:188. [PubMed: 17920217]
  21. Riley RR, Duensing S, Brake T, Munger K, Lambert PF, Arbeit JM. *Cancer Res.* 2003; 63:4862. [PubMed: 12941807]
  22. Sreekanth CN, Bava SV, Sreekumar E, Anto RJ. *Oncogene.* 2011; 30:3139. [PubMed: 21317920]
  23. Cairns RA, Hill RP. *Cancer Res.* 2004; 64:2054. [PubMed: 15026343]
  24. Thurber GM, Weissleder R. *PLoS One.* 2011; 6:e24696. [PubMed: 21935441]
  25. Minchinton AI, Tannock IF. *Nat Rev Cancer.* 2006; 6:583. [PubMed: 16862189]
  26. Schiffman M, Castle PE, Jeronimo J, Rodriguez AC, Wacholder S. *Lancet.* 2007; 370:890. [PubMed: 17826171]
  27. a) Ignatius AA, Claes LE. *Biomaterials.* 1996; 17:831. [PubMed: 8730968] b) Lu JM, Wang X, Marin-Muller C, Wang H, Lin PH, Yao Q, Chen C. Expert review of molecular diagnostics. 2009; 9:325. [PubMed: 19435455] c) Batrakova EV, Kabanov AV. *J Control Release.* 2008; 130:98. [PubMed: 18534704]
  28. Farokhzad OC, Cheng J, Teply BA, Sherifi I, Jon S, Kantoff PW, Richie JP, Langer R. *Proc Natl Acad Sci U S A.* 2006; 103:6315. [PubMed: 16606824]
  29. Yoo HS, Oh JE, Lee KH, Park TG. *Pharmaceutical Research.* 1999; 16:1114. [PubMed: 10450940]
  30. Harper E, Dang W, Lapidus RG, Garver RI Jr. *Clin Cancer Res.* 1999; 5:4242. [PubMed: 10632366]
  31. a) Catalone BJ, Kish-Catalone TM, Budgeon LR, Neely EB, Ferguson M, Krebs FC, Howett MK, Labib M, Rando R, Wigdahl B. *Antimicrob Agents Chemother.* 2004; 48:1837. [PubMed:

15105142] b) Costin GE, Raabe HA, Priston R, Evans E, Curren RD. *Altern Lab Anim.* 2011; 39:317. [PubMed: 21942546]

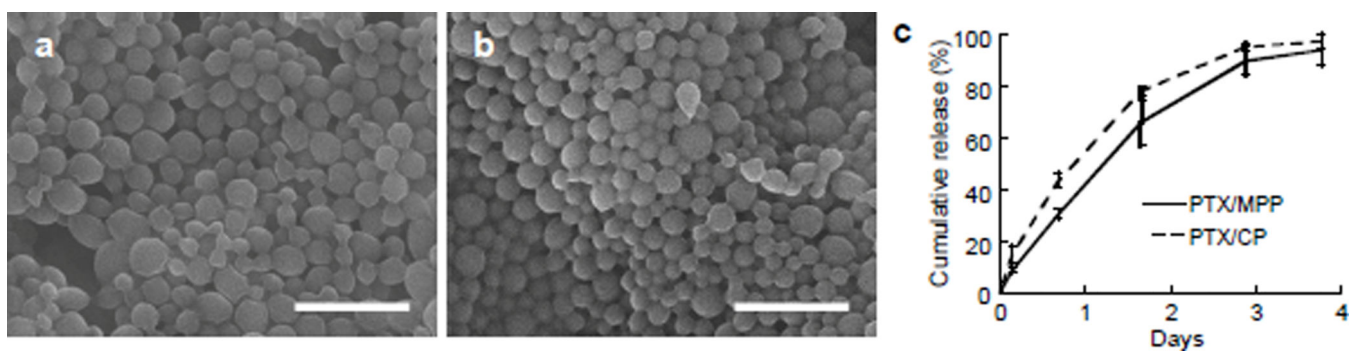


**Figure 1.** Characterization of PTX/PLGA nanoparticles *in vitro*. Scanning electron micrographs of PTX/MPP (a) and PTX/CP (b); scale bar represents 1  $\mu\text{m}$ . (c) Cumulative *in vitro* release of PTX from PTX/PLGA nanoparticles over time. Data represent the average values from two independent studies using different particle preparations. Error bars represent S.E.M.

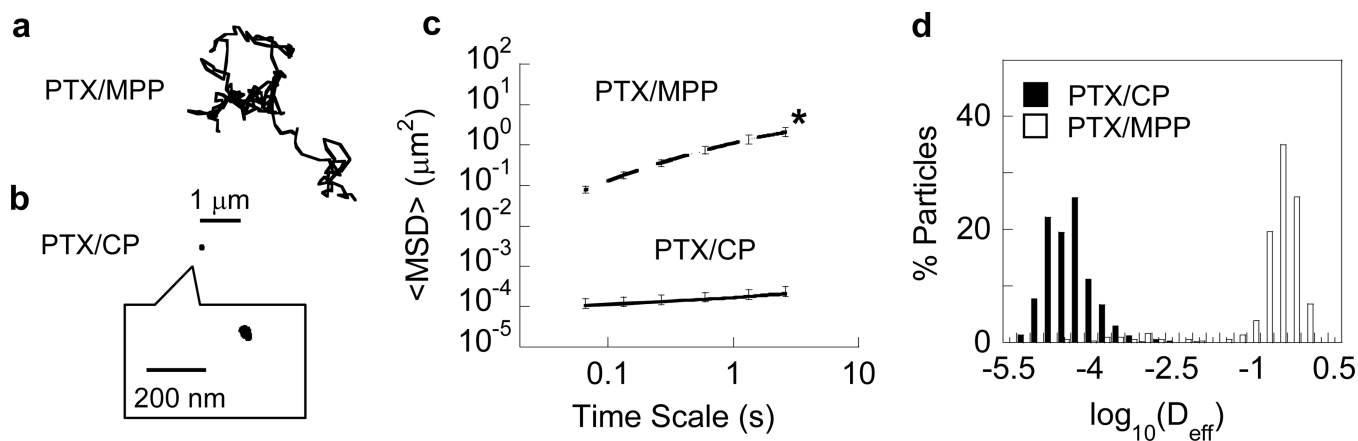


**Figure 2.** Transport of PTX-loaded PLGA particles in fresh human cervicovaginal mucus. Representative trajectories for (a) PTX/MPP and (b) PTX/CP, with effective diffusivities within one S.E.M. of the mean. (c) Ensemble-averaged geometric mean square displacements ( $\langle \text{MSD} \rangle$ ) as a function of time scale. Error bars represent S.E.M. \* indicates statistically significant difference across all time scales ( $p < 0.05$ ). (d) Distributions of the logarithms of individual particle effective diffusivities ( $D_{\text{eff}}$ ) at a time scale of 1 s. Data represent the average of at least three independent experiments, with  $n = 100$  per experiment for both PTX/MPP and PTX/CP.

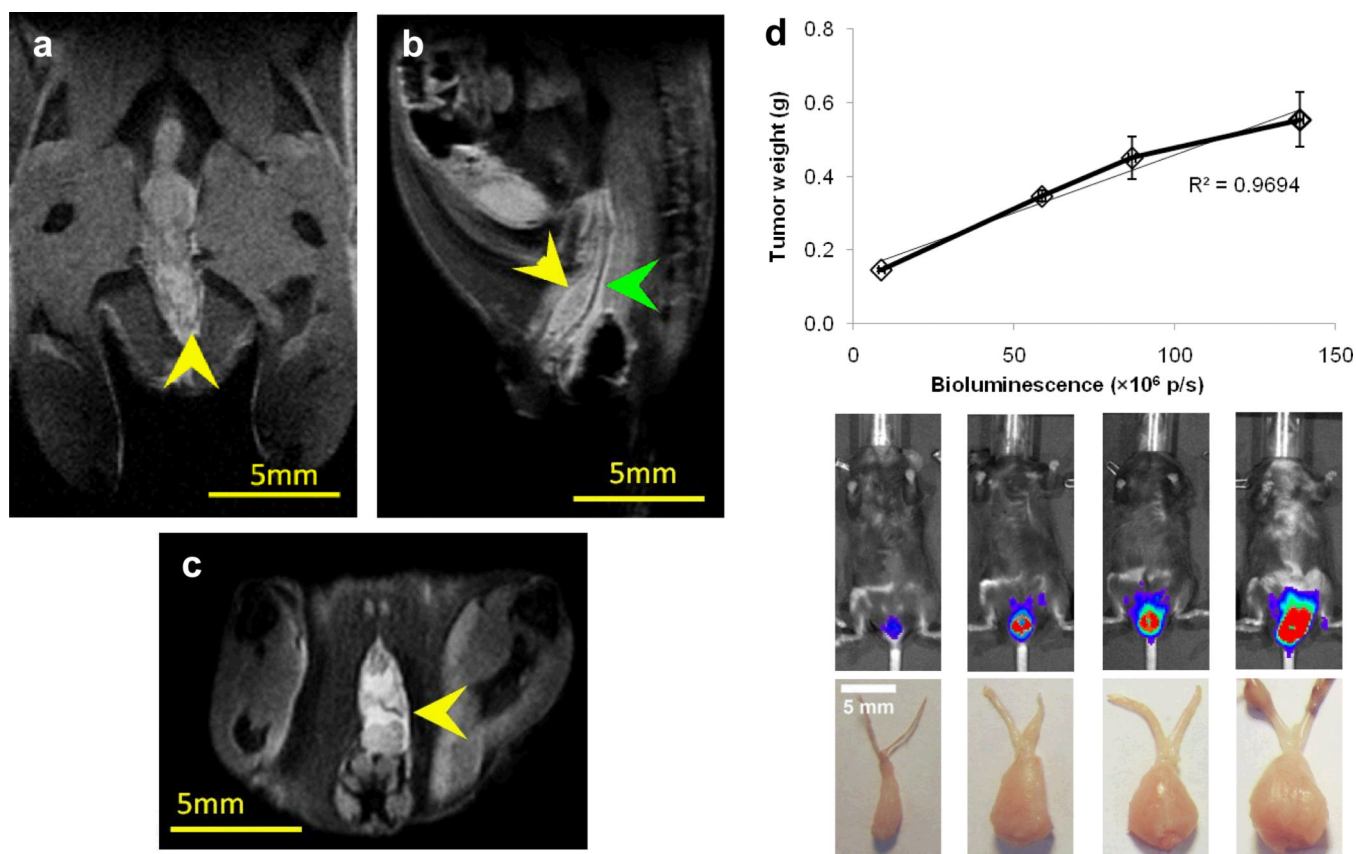


**Figure 3.** Magnetic resonance imaging (MRI) and bioluminescence imaging of TC-1 cervical tumors implanted in the mouse cervicovaginal tract. Representative coronal (**a**), sagittal (**b**), and axial (**c**) anatomical MR images of the female mouse reproductive tract, with yellow arrows indicating the location of the TC-1 tumor and the green arrow indicating the location of CV tract. The size of the tumor shown was measured to be 4.3 mm  $\times$  1.5 mm  $\times$  4.7 mm in the coronal, sagittal and axial directions, respectively. (**d**) Correlation of total bioluminescence and TC-1 tumor weight. Bioluminescence signals were quantified as the total photon flux (p/s, photons per second) of the tumor regions. The top row of images shows the tumor location and relative bioluminescence intensity, and the bottom row shows the physical appearance of the excised tumors. Error bars represent S.E.M. Scale bars represent 5 mm.

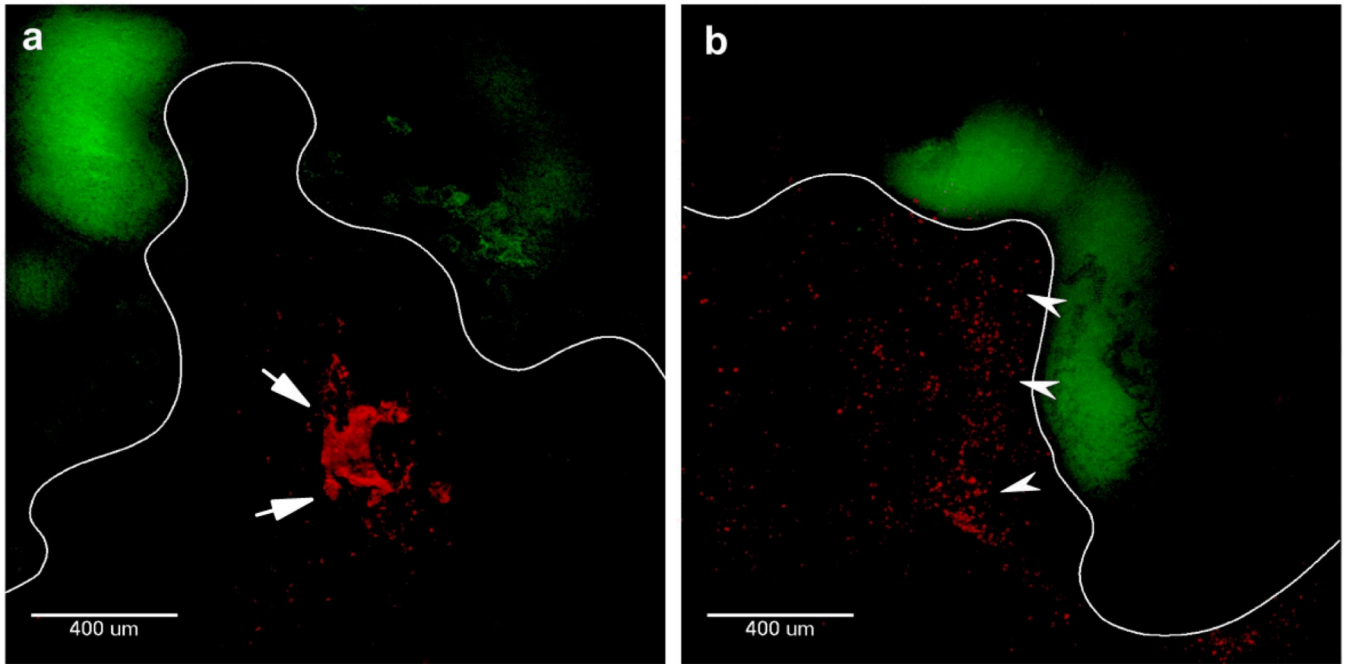


**Figure 4.** Transverse 50  $\mu\text{m}$  thick frozen sections of mouse vaginal tissue containing red fluorescent (a) PLGA CP or (b) PLGA MPP. Green corresponds to TC-1 cervical tumor expressing GFP. The epithelium is outlined in white to help distinguish the tissue surface. Arrows indicate the presence of large particle aggregates in the CV tract with PLGA CP in (a), while arrowheads indicate examples of well-dispersed PLGA MPP in (b). The same image acquisition and contrast settings were used for both images.

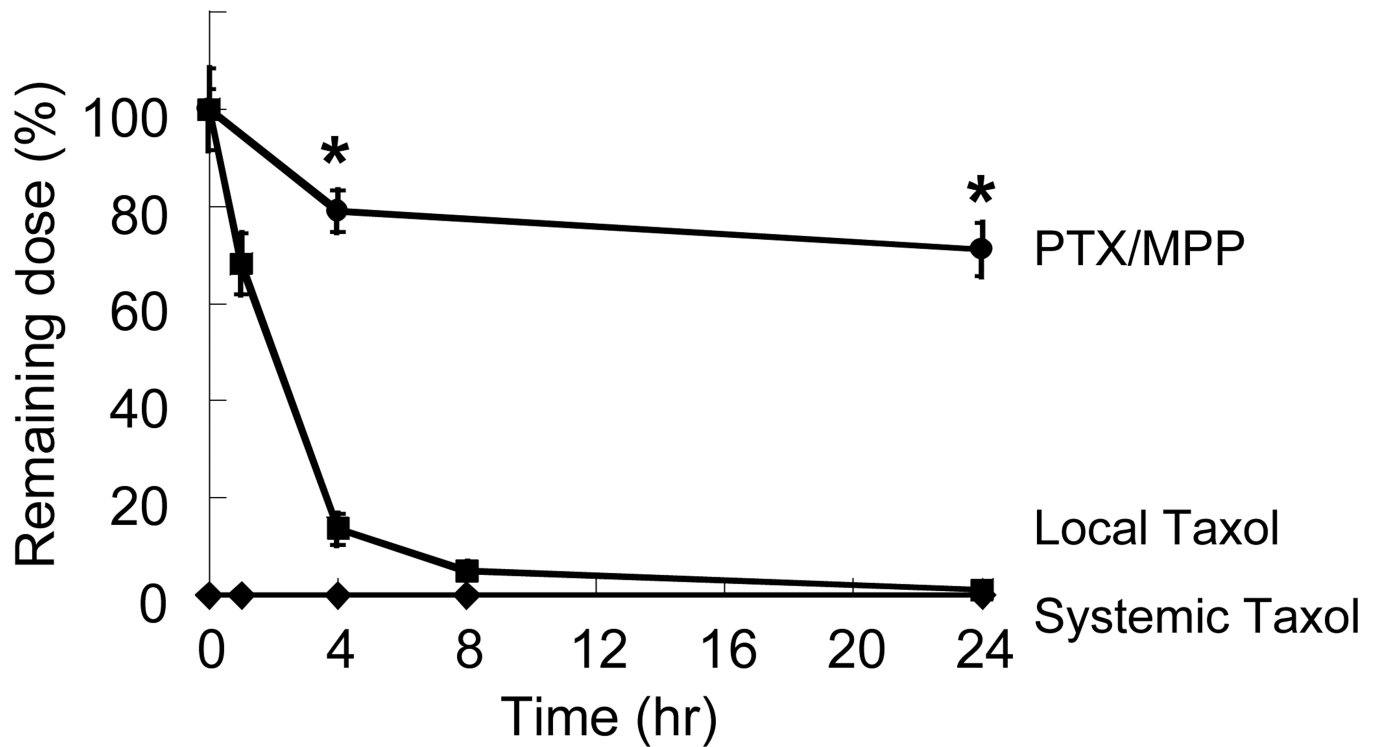


**Figure 5.**

Amount of PTX retained in the mouse CV tract over time, as delivered by PTX/MPP or as free drug by vaginal administration (local Taxol<sup>®</sup>) or by intraperitoneal administration (systemic Taxol<sup>®</sup>). The fraction of drug retained in the vagina is expressed as a percentage of the total amount of drug administered. \* indicates statistically significant difference compared to free drug at the same time point ( $p < 0.05$ ). Data represent at least  $n = 3$  mice per condition and time point. Error bars represent S.E.M.

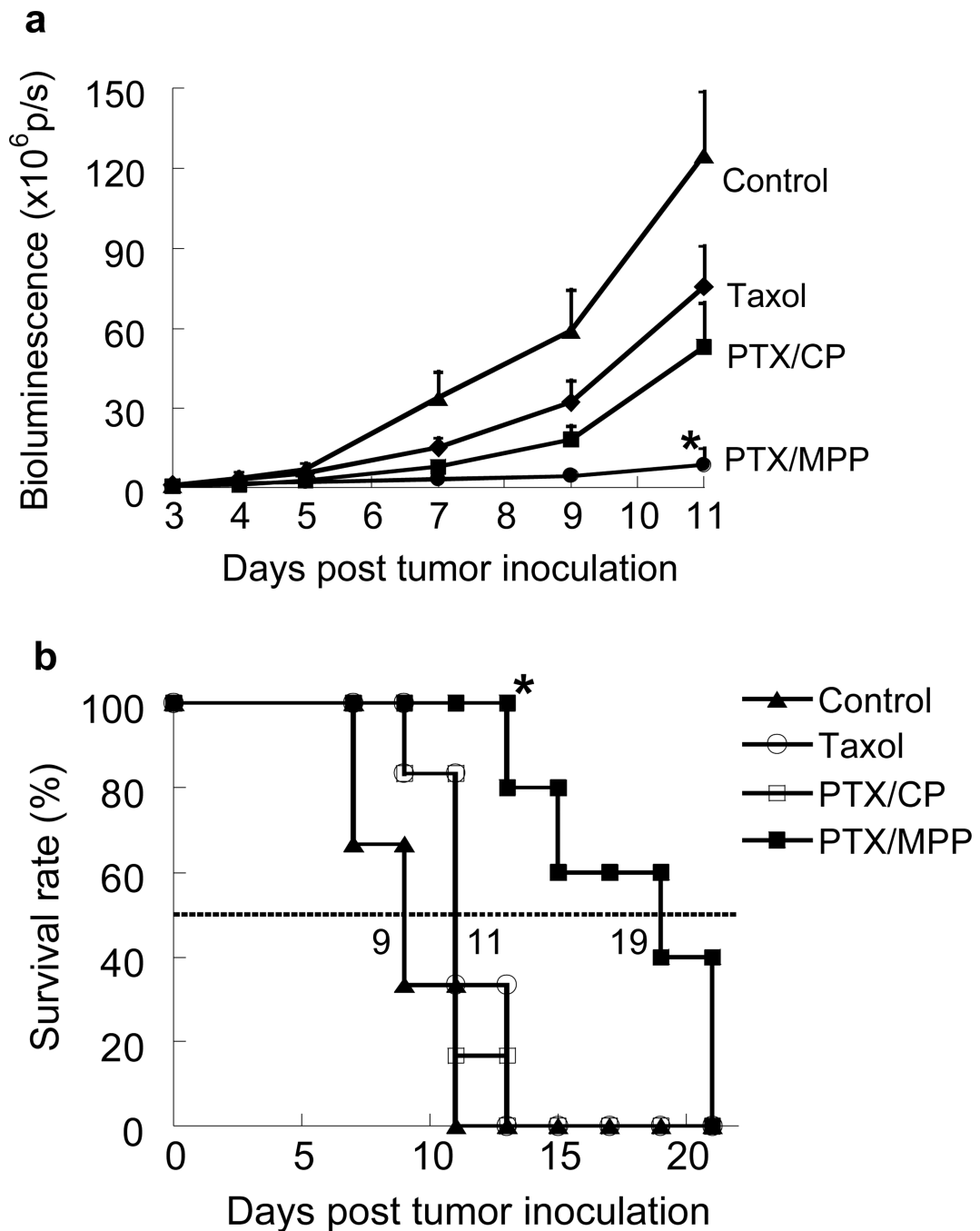


**Figure 6.** Response of TC-1 tumors established in the mouse cervicovaginal tract to local treatments with untreated control, free Taxol<sup>®</sup>, PTX/CP or PTX/MPP (n = 5–6 mice per treatment group). Tumors were inoculated on Day 0; treatments were given daily starting on Day 3. **(a)** Change in bioluminescence signal over the indicated time course. Signals were quantified as the total photon flux (p/s, photons per second) of the tumor regions. Error bars represent S.E.M. \* indicates significantly improved tumor suppression ( $p < 0.05$ ) compared to other treatments starting from Day 7. **(b)** Kaplan-Meier survival curves for mice bearing

cervicovaginal TC-1 tumors. \* indicates significantly improved survival rate ( $p < 0.05$ ) compared to other treatments starting from Day 13.

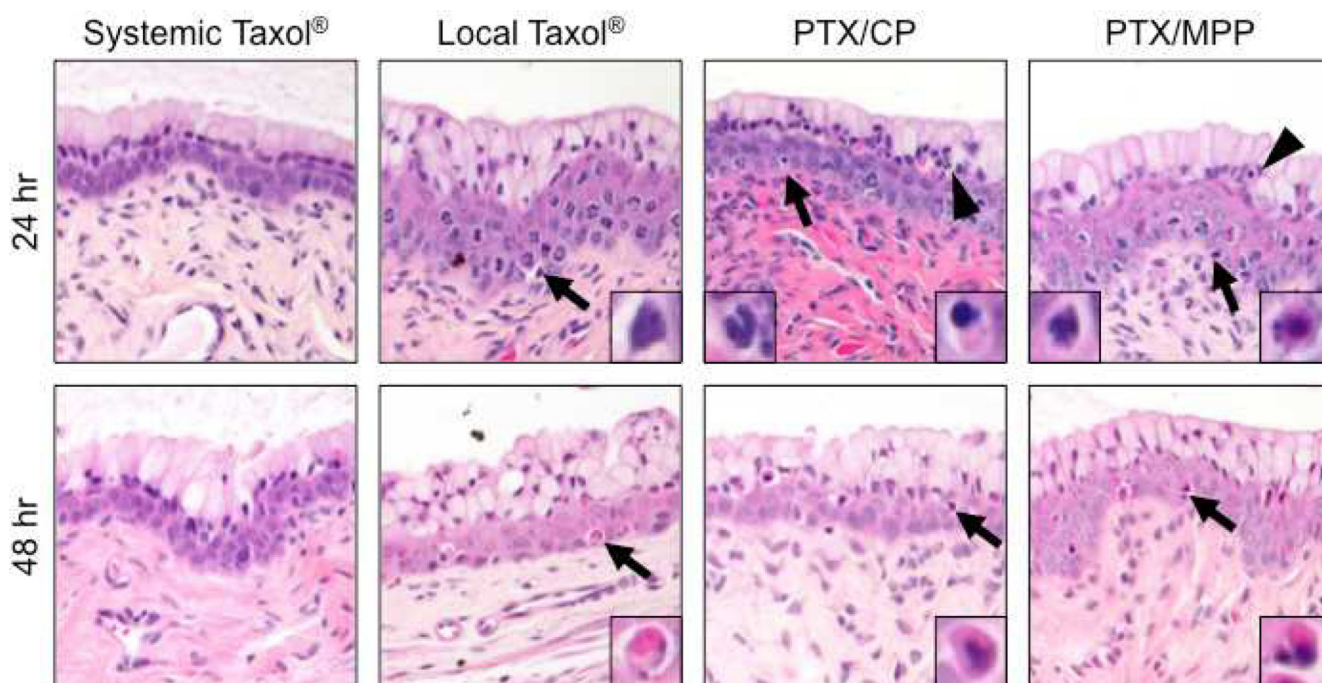


**Figure 7.** Histological sections of cervicovaginal tissue from mice treated with systemic Taxol<sup>®</sup>, local Taxol<sup>®</sup>, PTX/CP or PTX/MPP at 24 hr and 48 hr post administration (n = 5 mice per treatment group). Note the presence of pyknotic and apoptotic cells (arrows, right side inset) in local treatment groups at 24 hr and 48 hr, and inflammatory cells (arrowheads, left side inset) in PTX/CP and PTX/MPP treated mice at 24 hr.

**Table 1**

Characterization of PTX/ MPP and PTX/CP, and ratios of the ensemble average diffusion coefficients in water ( $D_w$ ) compared to in cervicovaginal mucus ( $D_m$ ).

| Formulation | Diameter [nm] | $\zeta$ -potential [mV] | Drug loading [%] | $D_w/D_m$ <sup>a)</sup> |
|-------------|---------------|-------------------------|------------------|-------------------------|
| PTX/ MPP    | 239 ± 5       | -7 ± 1                  | 5.2 ± 0.9        | 6                       |
| PTX/ CP     | 234 ± 4       | -1 ± 1                  | 8.7 ± 2.2        | 41,000                  |

<sup>a)</sup>Effective diffusivity values are calculated at a time scale of 1s.  $D_w$  is calculated from the Stokes-Einstein equation.